



# Performance of a Fe-N-C catalyst for the oxygen reduction reaction in direct methanol fuel cell: Cathode formulation optimization and short-term durability



Luigi Osmieri <sup>a,b,\*</sup>, Ricardo Escudero-Cid <sup>b</sup>, Alessandro H.A. Monteverde Videla <sup>a</sup>, Pilar Ocón <sup>b,\*</sup>, Stefania Specchia <sup>a</sup>

<sup>a</sup> Politecnico di Torino, Department of Applied Science and Technology, Corso Duca degli Abruzzi 24, 10129, Torino, Italy

<sup>b</sup> Universidad Autónoma de Madrid, Departamento de Química Física Aplicada, C/Francisco Tomás y Valiente 7, 28049, Madrid, Spain

## ARTICLE INFO

### Article history:

Received 16 June 2016

Received in revised form 28 July 2016

Accepted 16 August 2016

Available online 17 August 2016

### Keywords:

Non-noble metal catalyst

Iron-phthalocyanine

Oxygen reduction reaction

Rotating ring-disk electrode

Direct methanol fuel cell

## ABSTRACT

A non-noble metal (NNM) catalyst for oxygen reduction reaction (ORR) was synthesized using Fe(II)-phthalocyanine as unique source of Fe, N, and C, and SBA-15 ordered mesoporous silica as templating agent, resulting in a material with an extremely high specific surface area and a high microporosity (around 50%). FESEM, FTIR and Raman analyses were performed to investigate the morphology and the physicochemical properties of the catalyst. The ORR activity and the methanol tolerance were tested in rotating disk electrode (RDE), and the selectivity towards a complete 4-electrons reduction was investigated by rotating ring disk electrode (RRDE) test and hydrogen peroxide reduction test in RDE, showing very promising results. Thus, the Fe-N-C catalyst was tested at the cathode of a DMFC after determination of the optimal electrode formulation regarding catalyst loading and Nafion® content, showing a maximum power density of 20 mW cm<sup>-2</sup> at 90 °C. A short term durability test to assess the behavior of both the Fe-N-C and the Pt/C catalysts was conducted on the DMFC, showing a better performance of the non-noble catalyst. Thus, the Fe-N-C catalyst is a potential good candidate to be used as catalytic material for DMFC cathode, in alternative to Pt. The performance in a H<sub>2</sub>/O<sub>2</sub> PEMFC was tested as well, showing a power density of 105 mW cm<sup>-2</sup> at 60 °C.

© 2016 Elsevier B.V. All rights reserved.

## 1. Introduction

Polymer electrolyte membrane fuel cells (PEMFC) are efficient chemical-to-electrical conversion devices that can operate close to ambient conditions [1]. For this reason, they are suitable for portable and automotive applications [2]. Among PEMFC, direct methanol fuel cells (DMFC) have gained particular attraction for portable applications (*i.e.* as power supply units for electronic devices) [3] as alternative to Li-ion batteries, or for powering remote off-grid devices like environment monitoring stations and back-up units for telecommunications [4]. The main drawbacks of DMFC are represented by the use of Pt-based catalysts at both the anode and the cathode, and the methanol crossover through the

polymeric membrane, which dramatically affects both the durability and the performance [5]. Pt, in addition to its high cost [6], catalyzes both oxygen reduction reaction (ORR) and methanol oxidation reaction (MOR). Concerning ORR, high amounts of Pt are necessary at the cathode because of the sluggish kinetics of this reaction. On the other hand, concerning MOR, it is also a limiting step since Pt is poisoned by CO as reaction intermediate. Thus, the use of bimetallic Pt-Me (Me = Ru, Ir, Sn, Ni, etc.) is effective to reduce the CO poisoning effect [7]. Because of these problems, the research focused on the development of Pt-free catalysts for ORR [8]. Within several types of non-noble metal (NNM) catalysts for ORR, the most promising for low-temperature fuel cell application seem the carbon-supported transition metal/nitrogen (Me-N<sub>x</sub>/C) materials (Me = Co, Fe, Ni, Mn, etc.) [9,10]. They have gained increasing attention due to their promising catalytic activity towards ORR, along with the utilization of abundant and inexpensive precursor materials [11]. In fact, since from 1964 transition metal macrocyclic molecules like porphyrins and phthalocyanines were investigated as ORR electrocatalysts [12,13]. However, they showed stability problems, as the decomposition of their structure in acidic media,

\* Corresponding authors.

E-mail addresses: [luigi.osmieri@polito.it](mailto:luigi.osmieri@polito.it) (L. Osmieri), [ricardo.escudero@uam.es](mailto:ricardo.escudero@uam.es) (R. Escudero-Cid), [alessandro.monteverdevidela@polito.it](mailto:alessandro.monteverdevidela@polito.it) (A.H.A. Monteverde Videla), [pilar.ocon@uam.es](mailto:pilar.ocon@uam.es) (P. Ocón), [stefania.specchia@polito.it](mailto:stefania.specchia@polito.it) (S. Specchia).

resulting in a loss of catalytic activity. A significant breakthrough was achieved by performing a heat treatment at high temperature (600–1000 °C). During this heat treatment, a modification of the catalyst structure takes place, increasing the concentration of available ORR active ensembles while at the same time improving the catalyst stability [13,14]. Therefore, due to the modification of the structure after the high-temperature heat treatment, the use of transition metal macrocycle compounds was partially abandoned [15]. In fact, ORR active ensembles could also be formed starting from different precursors containing transition metals, nitrogen and carbon. For the production of ORR active ensembles, the presence of transition metal ions (Fe, Co, etc.), a source of carbon (carbon support, molecule, polymer), and a source of nitrogen (macrocycle, N-containing organic molecule or polymer, N-containing gas, i.e. NH<sub>3</sub>) are required during the heat-treatment [16].

To improve both activity and stability of NNM catalysts, several different approaches have been explored. Among them, the optimization of synthesis conditions and procedures, the development of heat-treatment strategies, the development of alternative carbon supports, and the use of different transition metal complexes with N-containing ligand molecules as precursors [17–19].

To increase the density of the active ensembles, and at the same time have a high specific surface area (to assure good mass transport properties), a possible synthesis approach lies in avoiding the use of a carbon support [20,21], using a non-carbonaceous sacrificial support with an ordered structure (e.g. silica, alumina, zirconia). This sacrificial support is mixed with the precursor(s) containing nitrogen, carbon and transition metal, and it is removed after the pyrolysis. The resulting material is a “self-supported” Me-N-C catalyst (Me = Fe, Co, etc.) obtained as a negative replica of the templating sacrificial agent. As a result, the self-supported Me-N-C catalyst has high pore volume and good accessibility to the active ensembles [22–24].

In addition to the above-mentioned properties, this type of Me-N-C catalysts show very promising methanol tolerance and they do not suffer CO poisoning [9,25–27]. In fact, one of the fundamental features of an NNM catalyst is the high methanol tolerance, to be considered attractive for DMFC applications, and to replace Pt-based catalysts at the cathode. However, one of the major issues that are still limiting the application of NNM catalysts in DMFC is the durability [28], whose decrease seems to be ascribed to both active ensembles deactivation and mass transport problems due to cathode flooding [21,29,30].

In this work, we synthesized a Fe-N-C catalyst by impregnation of Fe(II)-phthalocyanine (Fe-Pc) on SBA-15 silica used as a hard-templating agent, resulting in a material showing a high specific surface area, and extremely rich in microporosity. The ORR activity of this catalyst, and the selectivity towards a direct complete 4-electrons reduction to H<sub>2</sub>O, were assessed in a half-cell configuration by rotating disk electrode – rotating ring disk electrode (RDE-RRDE) technique, and performing a hydrogen peroxide reduction reaction (HPRR) test. Various MEA were prepared and tested in a 4 cm<sup>2</sup> single DMFC to optimize the Fe-N-C cathode formulation regarding catalyst loading and Nafion® content, and a short-term durability test in DMFC was performed. The performance of the Fe-N-C catalyst was assessed in an H<sub>2</sub>-fueled 4 cm<sup>2</sup> single PEMFC as well, for comparison purposes.

## 2. Experimental

### 2.1. Chemicals

Tetraethyl orthosilicate (TEOS, ≥ 98% purity), hydrochloric acid (HCl, 37 wt.%), Pluronic P123® triblock copolymer, hydrofluoric acid (HF, ≥ 40 wt.%), potassium hydroxide (KOH, 99.0% purity),

ethanol (≥ 99.8% purity), acetone (≥ 99.8% purity), isopropanol (≥ 99.7% purity), Nafion® 5 wt.% hydroalcoholic solution, and iron(II) phthalocyanine C<sub>32</sub>H<sub>16</sub>N<sub>8</sub>Fe (Fe-Pc, 90% purity) were purchased from Sigma-Aldrich. Vulcan XC72R (BET specific surface area of 250 m<sup>2</sup> g<sup>-1</sup>, average particle size of 40–50 nm) was donated by Cabot Corp. Nitrogen and oxygen gases were supplied in cylinders by SIAD with 99.999% purity. Ultrapure deionized water obtained from a Millipore Milli-Q system (resistivity > 18 MΩ cm) was used throughout the experiments. All reagents were used as received without further purification. 20 wt.% Pt/C (HiSPEC™ 3000, Pt 20 wt.% on carbon black, Johnson Matthey), 40 wt.% Pt/C (HiSPEC™ 4000, Pt 40 wt.% on carbon black, Johnson Matthey) and 30 wt.% PtRu/C (HiSPEC™ 5000, Pt-Ru 30 wt.% on carbon black, Pt:Ru atomic ratio = 1, Johnson Matthey) were purchased from Alfa Aesar.

### 2.2. Synthesis of Fe-N-C catalyst

SBA-15 silica used as templating agent for the preparation of Fe-N-C catalyst was prepared in-house following a procedure described elsewhere [31].

Fe-N-C catalyst was prepared using Fe-Pc precursor as a unique source of Fe, N, and C. The complete synthesis procedure is described in our previous work [32]. Briefly, Me(II)-phthalocyanine was dissolved in an ethanol-water solution and wet-impregnated on SBA-15 silica (SBA-15 to Fe-Pc wt. ratio 1:1). After solvent evaporation, a pyrolysis was performed under inert atmosphere (N<sub>2</sub> gas flow) at 800 °C for 1 h. Then, the SBA-15 silica was removed by washing with 5 wt.% HF solution.

### 2.3. Physicochemical characterization

A field emission scanning electron microscopy (FESEM, model JEOL JSM 6700F) was used to investigate the morphology of the SBA-15 silica and the Fe-N-C catalyst.

Fourier transform infrared spectroscopy (FTIR) analysis was conducted on the Fe-N-C catalyst. Before the measurement, the powder of Fe-N-C was mechanically mixed with KBr and pressed. IR spectra were collected in air at 2 cm<sup>-1</sup> resolution on a Bruker Equinox 55 FTIR spectrophotometer, equipped with an MCT (Mercury Cadmium Telluride) detector.

Raman spectroscopy was performed for the Fe-N-C catalyst to evaluate the ordered/disorder degree of its carbon-based crystalline structure, using a μ-Raman Spectroscopy μRS Renishaw InVia spectrometer equipped with a Leica DMLM confocal microscope and a CCD detector with an excitation wavelength of 785 nm (Renishaw plc, Gloucestershire, United Kingdom). The Raman scattered light was collected in the spectral range 100–1000 cm<sup>-1</sup>. At least ten scans were accumulated in four different positions of the catalyst to ensure a sufficiently high signal to noise ratio.

### 2.4. RDE-RRDE electrochemical tests

For RDE and RRDE tests on the Fe-N-C catalyst, the ink was prepared by mixing 10 mg of catalyst powder with 150 μL of H<sub>2</sub>O, 305 μL of isopropanol and 45.8 μL of Nafion 5% wt. solution. The ink was sonicated at 130 W for 30 min to achieve a good dispersion. With this formulation, the Nafion-to-catalyst mass ratio (NCR) is 0.2 and the catalyst density in the ink is 0.02 mg μL<sup>-1</sup>. 4 μL of ink were micropipetted on the glassy carbon surface of the RDE, resulting in a catalyst loading on the electrode of 637 μg cm<sup>-2</sup>.

As a comparison, a Pt catalyst (20 wt.% Pt/C) was also tested. In this case, the ink was prepared by dispersing 10 mg of catalyst (considering the total mass of Pt and C), 20 μL of deionized water, 33 μL of 5 wt% Nafion solution and 734 μL of isopropanol. The Pt loading on the electrode was 38 μg cm<sup>-2</sup>.

The electrochemical tests were performed in a three-electrodes cell, using a rotating disk electrode (RRDE-3A ALS) and a multi-potentiostat (Bio-Logic SP-150). The cell was equipped with a glassy carbon disk – platinum ring working electrode (disk diameter 4 mm, ring outer diameter 7 mm, ring inner diameter 5 mm), a platinum helical wire counter electrode, and a saturated calomel reference electrode (SCE). The electrolyte was a 0.5 M H<sub>2</sub>SO<sub>4</sub> solution (0.1 M HClO<sub>4</sub> for Pt/C catalyst), saturated with N<sub>2</sub> or O<sub>2</sub>. Before start tests, 50 cyclic voltammetry (CV) cycles at 100 mV s<sup>-1</sup> scan rate were performed in N<sub>2</sub>-saturated electrolyte. The last CV was recorded at 10 mV s<sup>-1</sup>.

For testing the ORR activity, a staircase voltammetry (SV) was recorded at 900 rpm RDE rotation speed in the O<sub>2</sub>-saturated electrolyte, with a potential step of 10 mV and a holding time at each potential of 30 s, to eliminate the capacitive current contribution. In this way, steady-state polarization curves were obtained [33].

From the linear portion of the potential vs. logarithm of current density plot (Tafel behavior), it is possible to calculate the Tafel slope and the exchange current density (*i*<sub>0</sub>) according to the Tafel Eq. (1):

$$E = E^0 + \frac{2.303RT}{\alpha_c F} \log i_0 - \frac{2.303RT}{\alpha_c F} \log i \quad (1)$$

where: *E* is the electrode potential, *E*<sup>0</sup> is the thermodynamic electrode potential of the ORR (1.23 V vs SHE), *R* is the universal gas constant (8.314 J mol<sup>-1</sup> K<sup>-1</sup>), *T* is the working temperature (K), *F* is the Faraday constant (96487 C mol<sup>-1</sup>),  $\alpha_c$  is the cathodic transfer coefficient, *i*<sub>0</sub> is the exchange current density, and *i* is the measured current density. According to Eq. (1), after having determined the slope (2.303RT/α<sub>c</sub>F) and the intercept (*E*<sup>0</sup> + (2.303RT/α<sub>c</sub>F) log(*i*<sub>0</sub>)) from the plot of *E* vs. log(*i*), the *i*<sub>0</sub> value can be calculated [34].

For the RRDE measurements, the rotation speed was 900 rpm, the disk potential was linearly varied at a scan rate of 5 mV s<sup>-1</sup>, and the ring potential was kept at 1.2 V vs RHE. The RRDE experiments were conducted using a bi-potentiostat (Mod. CH760E). The background current measured at the ring at potentials higher than the reaction onset (above 0.83 V and 0.95 vs RHE for Fe-N-C and Pt/C, respectively) was subtracted from the ring signal throughout the whole scanned potential range [35].

The electro-reduction of H<sub>2</sub>O<sub>2</sub> (HPRR) in the absence of O<sub>2</sub> was assessed for the Fe-N-C catalyst performing a linear sweep voltammetry (LSV) at 5 mV s<sup>-1</sup> and 1600 rpm in N<sub>2</sub>-saturated 0.5 M H<sub>2</sub>SO<sub>4</sub> solution after the addition of H<sub>2</sub>O<sub>2</sub> in the concentration of 1 mM. A LSV in O<sub>2</sub>-saturated 0.5 M H<sub>2</sub>SO<sub>4</sub> solution at 1600 rpm was also recorded to compare ORR with HPRR.

The ORR polarization curves in the presence of methanol (methanol tolerance test) were measured performing LSV at 5 mV s<sup>-1</sup> and 900 rpm in 0.5 M H<sub>2</sub>SO<sub>4</sub> saturated with O<sub>2</sub>. Methanol was progressively added in a concentration of 0.01, 0.1, 1, and 2 M. The cell was equipped with a saturated Ag/AgCl reference electrode, a graphite rod counter electrode and a glassy carbon disk with a diameter of 5 mm (RDE PINE) as working electrode. The 20 wt.% Pt/C commercial catalyst was also tested in the presence of methanol (0.1 M) for comparison.

All the measurements were performed at room temperature, and the electrode potentials were referred to the reversible hydrogen electrode (RHE). The current densities were normalized to the geometric area of the glassy carbon disk electrodes.

## 2.5. Single PEMFC test (H<sub>2</sub>/O<sub>2</sub> and DMFC)

The Fe-N-C catalyst performance as ORR cathodic catalyst was evaluated in a 4 cm<sup>2</sup> single DMFC. A Nafion® 117 membrane (Dupont) was used as the electrolyte. This membrane is thicker than others used in other DMFC studies with similar NNM catalysts (that are methanol tolerant) [9,25,36], however it is typically

used when Pt/C is used as cathodic catalyst to limit the detrimental crossover effect. To better compare the performance of our Fe-N-C catalyst with the commercial Pt/C, this thicker membrane was chosen for the DMFC test in this work.

Before use, the membrane was protonated following a procedure described elsewhere [37]. A commercial Pt-Ru catalyst (30 wt.% Pt-Ru/C) was used as anodic catalyst. A commercial Pt catalyst (40 wt.% Pt/C) at the cathode was also evaluated.

The electrodes were prepared by spraying the catalyst ink onto a gas diffusion layer (ELAT GDL-LT 1200 W). The inks were prepared by mixing the catalysts powder with an isopropanol/deionized water solution (2:1 vol.) and an adequate amount of Nafion® ionomer solution (5 wt.%). The Nafion® solution amount was in accordance with the desired amount of ionomer in the dry catalytic layer. Electrodes with a Nafion® content of 4, 35, 50, and 66 wt.% were prepared, while the Fe-N-C catalyst loadings used were 2.5 and 5 mg cm<sup>-2</sup>. For Pt-Ru and Pt-based electrodes, the Pt loading on the electrodes was set to 1 mg cm<sup>-2</sup>, with a Nafion® content of 4 wt.% on the dry electrode, according to our previous work [38] and other literature works [39,40].

The membrane electrode assembly (MEA) was obtained by hot pressing at 100 °C and 60 bar for 3 min.

For the DMFC test, the MEA was mounted into a 4 cm<sup>2</sup> single cell (Electrochem Inc.). The thickness of the gaskets used was 0.3 mm. A fuel cell test bench (MITS Pro-FCTS, Arbin Instruments, USA) was used for the evaluation. The DMFC anodic compartment was fed with 2 M methanol solution preheated at 80 °C with a flow rate of 1 mL min<sup>-1</sup> and a pressure of 0.33 bar (relative). The cathodic compartment was fed with a 200 NmL min<sup>-1</sup> pure O<sub>2</sub> flow preheated at 80 °C, with a backpressure of 3 bar and no humidification. The cell temperature was 90 °C. The polarization curve was recorded at 10 mV s<sup>-1</sup> from open circuit potential (*E*<sub>oc</sub>) down to 0.0 V. A short-term durability test, consisting in keeping the potential constant for 3 h at 0.4 V, was conducted in the same operating conditions described above, with a flow rate of the methanol solution at the anode of 5 mL min<sup>-1</sup> [41]. A polarization curve was recorded every 30 min.

The Fe-N-C catalyst performance was also tested in a PEMFC using H<sub>2</sub> as fuel. The same 4 cm<sup>2</sup> active area single cell and the same gaskets were used. In this case, a commercial Nafion® 112 membrane (Dupont) was used. Before use, the membrane was pre-treated as described previously for Nafion® 117 membranes. The Fe-N-C cathode was prepared using a Nafion® content on the dry electrode of 50 wt.% and a catalyst loading of 2.5 mg cm<sup>-2</sup>. At the PEMFC anode, a commercial Pt catalyst (40 wt.% Pt/C) with a Pt loading of 0.3 mg cm<sup>-2</sup> was used. As a purpose of comparison, the performance of a PEMFC prepared using a commercial Pt catalyst (40 wt.% Pt/C) with a Pt loading of 0.6 mg cm<sup>-2</sup> at the cathode was also evaluated. In the case of Pt/C catalyst, the Nafion® content on the dry electrode was 4 wt.% for both anode and cathode. The anodic and cathodic compartments were fed with a 200 NmL min<sup>-1</sup> H<sub>2</sub> (fully humidified) and O<sub>2</sub> (without humidification) flow, respectively. For both H<sub>2</sub> and O<sub>2</sub> the backpressure was 3 bar. The temperature of the cell was kept at 60 °C during the experiments, according to our previous work [42].

## 3. Results and discussion

### 3.1. Physicochemical characterization

A detailed physicochemical characterization of the Fe-N-C catalyst is reported in our previous work [32]. To briefly summarize, this catalyst has a BET specific surface area of 1508 m<sup>2</sup> g<sup>-1</sup>, of which 48% is given by micropores. The bulk Fe content (measured by EDX) is 0.64 at.%, and the Fe content on the catalyst surface (measured by

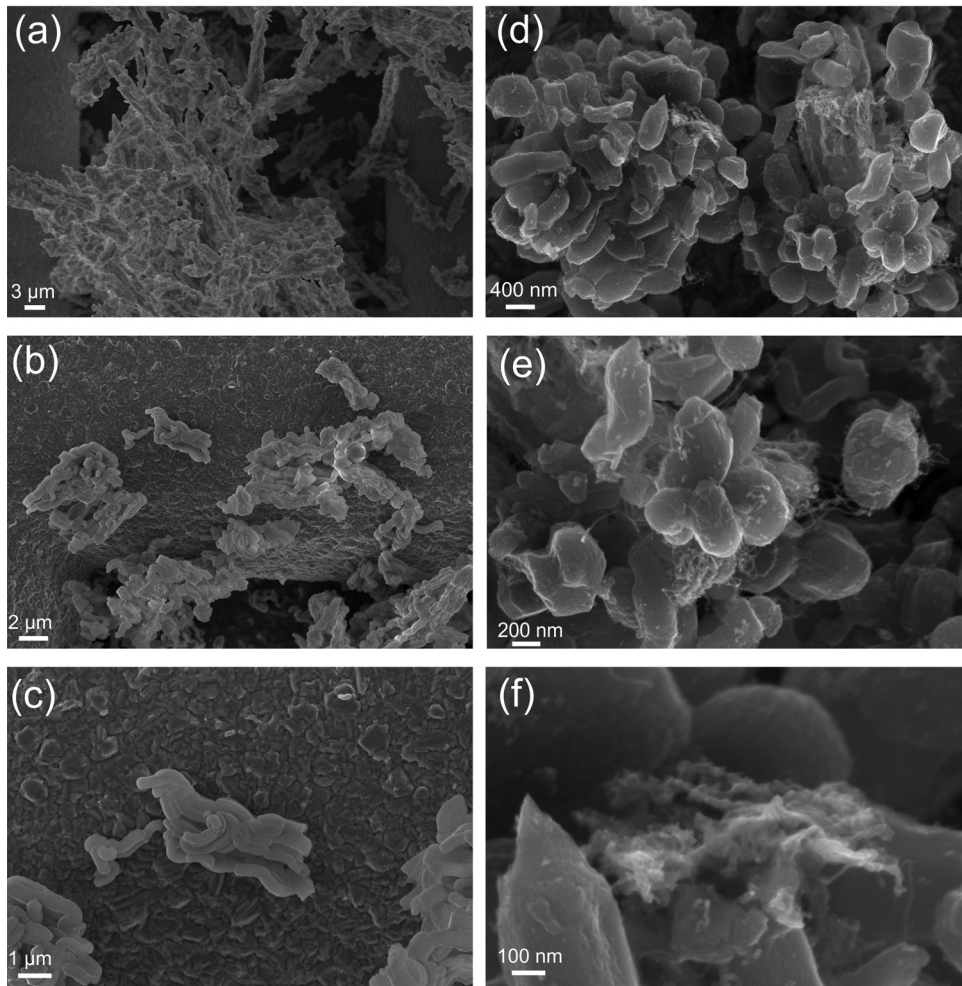


**Fig. 1.** FESEM images at different magnifications of SBA-15 silica (a–b–c) and Fe-N-C catalyst (d–e–f).

XPS) is 0.1 at.%. The overall surface N content was also determined by XPS and is of 5.0 at.%. This total N content is constituted by a 12.5% of nitrile-N, 26.9% of pyridinic-N, 2.0% of Fe-N<sub>x</sub> moieties, 41.6% of graphitic- and/or pyrrolic-N, and 17.0% of oxidized-N (determined by deconvolution analysis of the XPS N 1 s peak).

### 3.1.1. FESEM

Fig. 1a–b–c show FESEM pictures of SBA-15 silica used as templating agent. The SBA-15 silica has the typical uniform rod-like morphology [43–45]. These worm-shaped rod particles have a length of about 1  $\mu$ m and a diameter of about 200 nm, and they are joined to form larger agglomerates, which is typical of SBA-15 silica. Fig. 1d–e–f show the pictures of the Fe-N-C catalyst. As evident, it also has a rod-like morphology, similarly to the silica template. In the literature as well there are many examples of materials with similar rod-like morphology, synthesized via the same hard-templating method of SBA-15 silica [46,47]. Considering the dimensions of the worm-shaped rods of Fe-N-C, the average particles diameter is similar to the SBA-15 (about 200 nm), while the average length is lower compared to that of SBA-15. To explain this effect, we could consider that the ordered channel-like pores of the SBA-15 silica lie along the length direction. Thus, the lower length of the Fe-N-C catalysts particles can be a consequence of an incomplete filling of the empty space inside the channels by the Fe-Pc precursor during the impregnation. In this way, the negative replica of the template occurred only partially along the channel-

like pores length direction, originating shorter particles after the silica template removal.

Moreover, the Fe-N-C catalyst has a composite morphology where different zones can be identified (see Fig. 1d–f). In facts, the rod-like particles originated as a replica of the SBA-15 are surrounded and interconnected by a less uniform and disordered structure. Observing the image at higher magnification (Fig. 1f), this disordered region seems to be formed by root-like filaments, similar to agglomerates of short nanotubes. The presence of longer nanotubes interconnecting the different rod-like particles is evident in the pictures at lower magnifications (Fig. 1d–e).

### 3.1.2. FTIR analysis

FTIR analysis was performed on the Fe-Pc precursor before pyrolysis, and on Fe-N-C catalyst after pyrolysis and silica template removal. Fig. 2a shows the resulting spectra.

FTIR spectrum of Fe-Pc shows stretching and bending vibration bands typical of phthalocyanines [22,48]: C–H stretching (3054  $\text{cm}^{-1}$ ) and C–C stretching (1607  $\text{cm}^{-1}$ ) of aromatic rings, –N=N– mesoatoms stretching (1513  $\text{cm}^{-1}$ ); isoindole (1422  $\text{cm}^{-1}$ ) and pyrrole (1331  $\text{cm}^{-1}$ ) stretching, in-plane (1287, 1163, 1081  $\text{cm}^{-1}$ ) and out-of-plane (734, 780  $\text{cm}^{-1}$ ) bending of C–H in aromatic rings.

After pyrolysis, most of the peaks characteristic of the phthalocyanine molecule in the “fingerprint” wavenumber region between 1700 and 700  $\text{cm}^{-1}$  disappear. In facts, the spectrum of Fe-N-C catalyst is similar to the typical spectrum of carbonaceous mate-

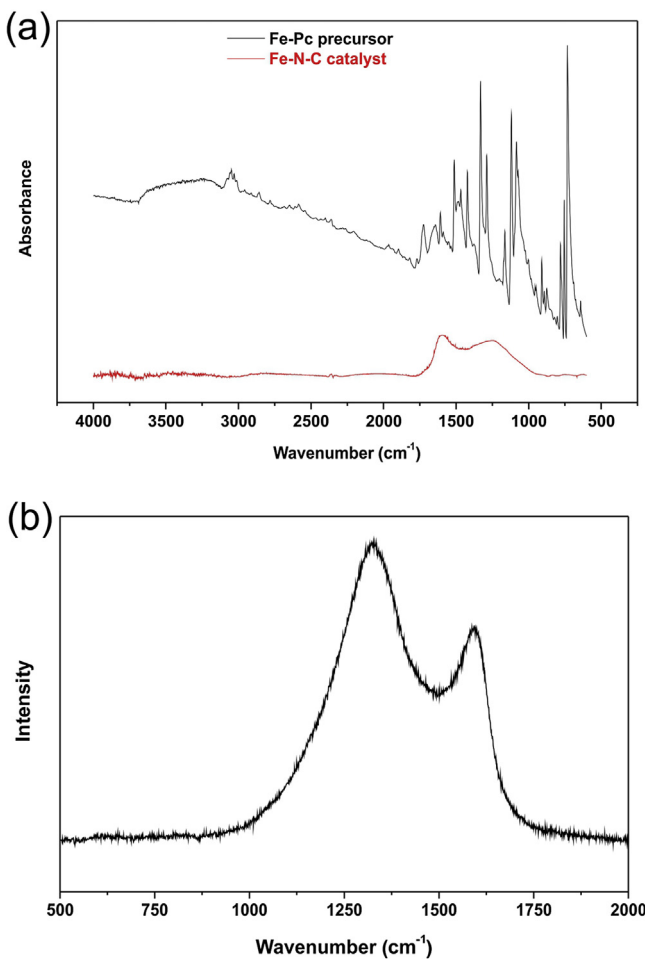


**Fig. 2.** (a) FTIR spectra of the Fe-N-C catalyst after the silica template removal and of the Fe(II)-phthalocyanine molecule precursor of the catalyst before pyrolysis. (b) Raman spectrum of Fe-N-C catalyst.

rials, which are highly transparent to the IR radiation in the region between 400 and 4000 cm<sup>-1</sup> [47]. The FTIR spectrum of Fe-N-C catalyst exhibits only two broad absorbance peaks in the ranges 1650–1500 cm<sup>-1</sup> and 1350–1150 cm<sup>-1</sup>. These peaks can be attributed to C=N bonds (i.e. pyridine-type) and N–H bonds that can be found on N-containing carbon materials [49]. Similar results are available in the literature for different types of pyrolyzed Me-N-C electrocatalysts [50,51]. This suggests that the original phthalocyanine structure of the precursor decomposes totally during the pyrolysis process, with a substantial recombination of the chemical bonding [32].

### 3.1.3. Raman analysis

The Raman spectra were recorded to evaluate the order/disorder degree of the carbon crystalline structure of the Fe-N-C catalyst. The *D* band (with peak intensity at ~1300 cm<sup>-1</sup>) corresponds to disordered carbon or defective graphitic structures, while the *G* band (with peak intensity at ~1600 cm<sup>-1</sup>) is a characteristic feature of graphitic layers [49]. Fig. 2b shows the results. The ratio between the intensities of the *D* band and the *G* band ( $I_D/I_G$ ) allows the estimation of the ratio between the disordered and the graphitic carbon structure of the catalyst. Therefore, a high  $I_D/I_G$  band intensity ratio points out the presence of high amounts of defects [52]. These defects can be caused by the incorporation of hetero-atoms (e.g., nitrogen or oxygen) or of *sp*<sup>3</sup>-hybridized carbon atoms in *sp*<sup>2</sup> grapheme lattices [10,53,54].

No presence of any additional peak between the *G* and *D* band, attributable to incomplete carbonization [49], was detected for these catalysts, suggesting that the Fe-Pc precursor got a good degree of carbonization during the pyrolysis process. In particular, during the heat treatment at high temperature under inert atmosphere, two phenomena take place: i. the precursor graphitization forming a carbonaceous structure, and ii. the simultaneous doping of this structure with some of the N atoms present in the precursor molecule [10]. The former is responsible for the electronic conduction of the material, and the latter of the formation of the ORR active ensembles.

The graphitization process leads to a lower  $I_D/I_G$  ratio [55], while the doping with nitrogen causes an increase of defects in the carbon phase. The latter, in turns, causes an increase in the  $I_D/I_G$  ratio, as well as a broadening of the *D* and *G* peaks [56]. Thus, the final value of the  $I_D/I_G$  ratio is the net effect of the sum of its decrease due to further graphitization and its increase due to nitrogen introduction in the structure. The  $I_D/I_G$  ratio for Fe-N-C catalyst calculated from Fig. 2b is 1.215. This value is high compared to the values between 0.7 and 1.1 reported in the literature for carbonaceous materials and N-doped and Fe-N-doped C-based materials [10,11,57,58]. Higher  $I_D/I_G$  ratio values are usually ascribed to the incorporation of N and Fe in the graphitic structure of the C-support. This result can be explained by the high heteroatom-doping level resulting in the carbonaceous matrix structure of the Fe-N-C after the pyrolysis, as confirmed by XPS [32] and by FTIR analysis.

### 3.2. RDE-RRDE electrochemical characterization

Before recording the CV, the catalysts were first cycled in N<sub>2</sub> saturated solution at 100 mV s<sup>-1</sup> until stable response. Fig. 3a shows the CV recorded at 10 mV s<sup>-1</sup>. The small contribution of redox peaks of Fe<sup>2+</sup>/Fe<sup>3+</sup> or quinone/hydroquinone surface groups at around 0.3–0.8 V vs. RHE is observable. The specific capacitance of Fe-N-C was calculated according to the procedure reported by Jaouen et al. [59]. The specific capacitance was 128.5 F g<sup>-1</sup>, comparable to the values showed by other Fe-N-C-based NNM catalysts reported in the literature [59,60]. The capacitive current exhibited in the N<sub>2</sub>-saturated electrolyte can be ascribed to both the extremely high specific surface area of this material (~1500 m<sup>2</sup> g<sup>-1</sup>) [32] and the surface functionalization with O- and N-containing functional groups. In particular, the specific surface area is related to the double layer interface, which, in turn, is related to the electrostatic double layer capacitance. Otherwise, the surface functionalization is responsible for the enhancement of the pseudocapacitive phenomena, that is, quick faradaic charge transfer reactions occurring at the double layer [61,62].

The ORR process is diffusion-controlled at potentials more negative than 0.5 V vs. RHE, where the curves show a current density plateau, which increases with the rotation rate (200–3600 rpm, not reported here). A mixed diffusion-kinetic control appears in the potential region between 0.5 and 0.7 V vs. RHE and at more positive potentials, kinetic control dominates being independent of the rotation rate.

Fig. 3b shows the comparison between ORR activity of Fe-N-C with the commercial 20 wt.% Pt/C catalyst. The Fe-N-C catalyst exhibits a high overpotential in comparison with Pt/C (in both anodic or cathodic scan), but it is interesting the comparison with the kinetic parameters such as Tafel slope and exchange current density ( $i_0$ ). The kinetic current  $i_k$  was calculated using Equation (2), to eliminate the effects of the mass transport limitation [63]:

$$i_k = - \frac{i_L \cdot i}{i_L - i} \quad (2)$$

where:  $i_k$  is the mass transport-corrected current density,  $i$  is the measured current density, and  $i_L$  is the limiting current density

**Table 1**

ORR kinetic parameters for the Fe-N-C catalyst and the Pt/C commercial catalyst (in anodic and cathodic scan direction). LO = low overpotential region; HO = high overpotential region.

Sample	$E_{on}$ [V vs RHE]	$E_{1/2}$ [V vs RHE]	Tafel slope LO [mV dec $^{-1}$ ]	$i_0$ LO [mA cm $^{-2}$ ]	Tafel slope HO [mV dec $^{-1}$ ]	$i_0$ HO [mA cm $^{-2}$ ]
Fe-N-C	0.83	0.72	64	$5.14 \times 10^{-8}$	141	$8.67 \times 10^{-4}$
Pt cath scan	0.87	0.76	60	$1.41 \times 10^{-7}$	202	$3.63 \times 10^{-2}$
Pt anod scan	0.93	0.82	63	$2.30 \times 10^{-6}$	126	$3.93 \times 10^{-3}$

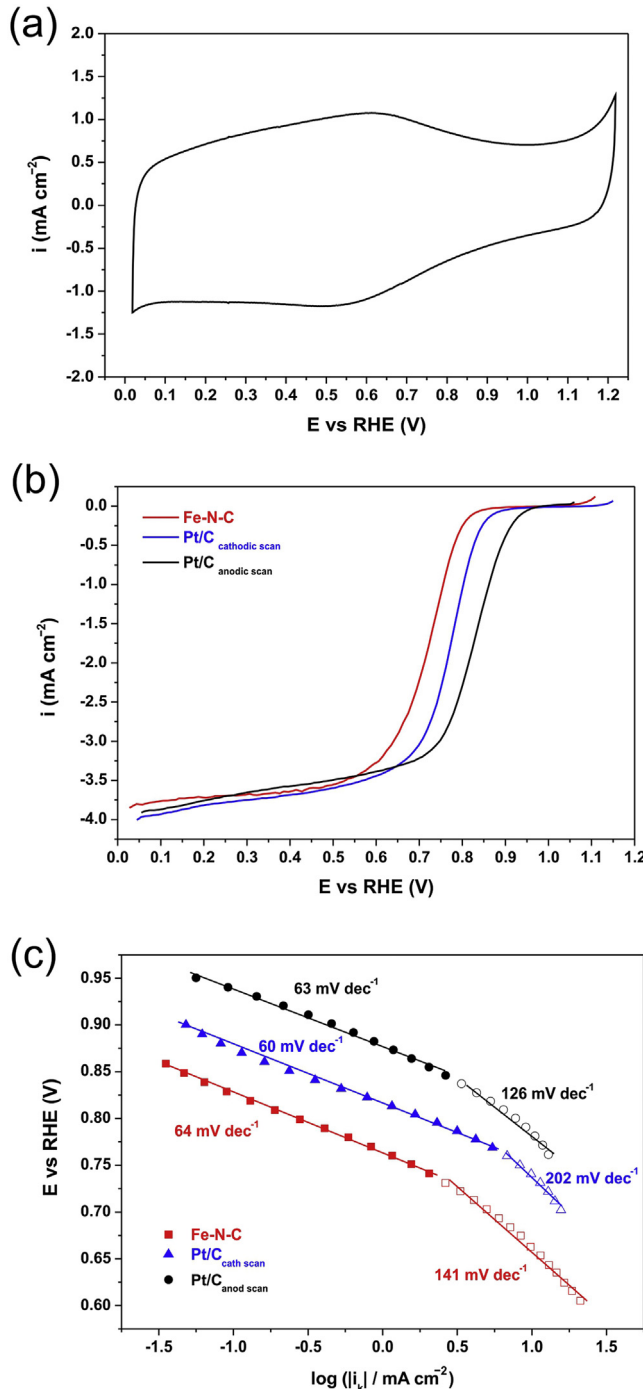


**Fig. 3.** (a) Cyclic voltammetry of Fe-N-C catalyst recorded in  $\text{N}_2$ -saturated 0.5 M  $\text{H}_2\text{SO}_4$  solution at 10 mV s $^{-1}$  potential scan rate and catalyst loading of 0.64 mg cm $^{-2}$ . (b) Staircase voltammetry of Fe-N-C catalysts (red) recorded in  $\text{O}_2$ -saturated 0.5 M  $\text{H}_2\text{SO}_4$  at 900 rpm and of a Pt catalyst (20 wt.% Pt/C) in  $\text{O}_2$ -saturated 0.1 M  $\text{HClO}_4$  in both cathodic (blue) and anodic (black) scan direction. (c) Tafel plot derived from data in (b). (For interpretation of the references to colour in this figure legend, the reader is referred to the web version of this article.)

measured in the plateau region of the polarization curve at high overpotential. Fig. 3c shows the Tafel plots derived from these data. Table 1 lists the calculated ORR kinetic parameters, such as Tafel slopes and exchange current densities.

In the Tafel plots of Fig. 3c, for Fe-N-C and Pt/C catalyst (in both anodic and cathodic scan directions) two different Tafel slope zones can be identified. The first zone appears at low overpotentials (LO) (approximately: 0.85–0.75 V vs. RHE for Fe-N-C; 0.90–0.80 V vs. RHE for Pt/C cathodic scan; 0.95–0.85 V vs. RHE for Pt/C anodic scan). The second zone appears at higher overpotentials (HO) (approximately: 0.75–0.60 V vs. RHE for Fe-N-C; 0.80–0.70 V vs. RHE for Pt/C cathodic scan; 0.85–0.75 V vs. RHE for Pt/C anodic scan).

For Fe-N-C, at LO the Tafel slope is around 60 mV dec $^{-1}$ , and at HO the slope increases more than two-fold, becoming 140 mV dec $^{-1}$ , and the linear trend is less evident, suggesting a changing in the reaction mechanism occurring in this zone [64]. An analogous two-slope behavior can be found in the literature in acid conditions for NNM catalysts based on Fe, N, and C [64]. In this regard, the behavior of the Fe-N-C catalyst can be compared with the Pt-based catalysts. In fact, it is widely reported in the literature that the measured Tafel slope for single crystal Pt electrodes [65], polycrystalline Pt [66] and carbon supported Pt catalysts [67] suffers a shift from about 60 mV dec $^{-1}$  at low overpotentials to 120 mV dec $^{-1}$  at higher overpotentials [68,69]. This effect is explained for Pt by surface active sites partial blocking by oxygen-containing reaction intermediates varying with the potential. It influences the reaction rate at small overpotentials even when the removal of the intermediates involves fast quasi-equilibrium steps, and if the initial electron transfer is the rate-determining step (RDS) of the reaction over the whole potential range considered.

In particular, the change of the Tafel slope from 60 to 120 mV dec $^{-1}$  at high currents at Pt surface (both Pt smooth surface and small Pt particles) is explained by the change in Temkin to Langmuir adsorption conditions (i.e., by the decrease in the surface coverage) but not by the change in the RDS [70–74]. The coupling of such equilibrium processes to the rate-limiting step leads to a coverage-dependent, and hence potential-dependent apparent Tafel slope [68].

When estimating ORR activity for Pt-based catalysts, usually the anodic scan direction is analyzed as, in this case, activity is not affected by an oxide layer, which is slowly removed when the potential is decreasing. Analyzing both the anodic and cathodic sweep directions, a certain hysteresis is observed in the polarization curve (see Fig. 3b). This is commonly ascribed to slow removal of surface oxides which hinders ORR during negative going sweep [75].

Other important parameters which define the performance of an ORR catalyst are the onset potential ( $E_{on}$ ) and the half-wave potential ( $E_{1/2}$ ).  $E_{on}$  is defined as the potential required to generate a current density of 0.1 mA cm $^{-2}$  in a steady-state RDE experiment [51], and  $E_{1/2}$  is the potential required to have half the maximum current density in the polarization curve.

As summarized in Table 1, the Fe-N-C catalyst exhibits a 100 mV negative shift in both  $E_{on}$  and  $E_{1/2}$  compared to the Pt/C commercial catalyst (considering the anodic scan direction). Even if these values are lower than the best “state-of-the-art” catalysts

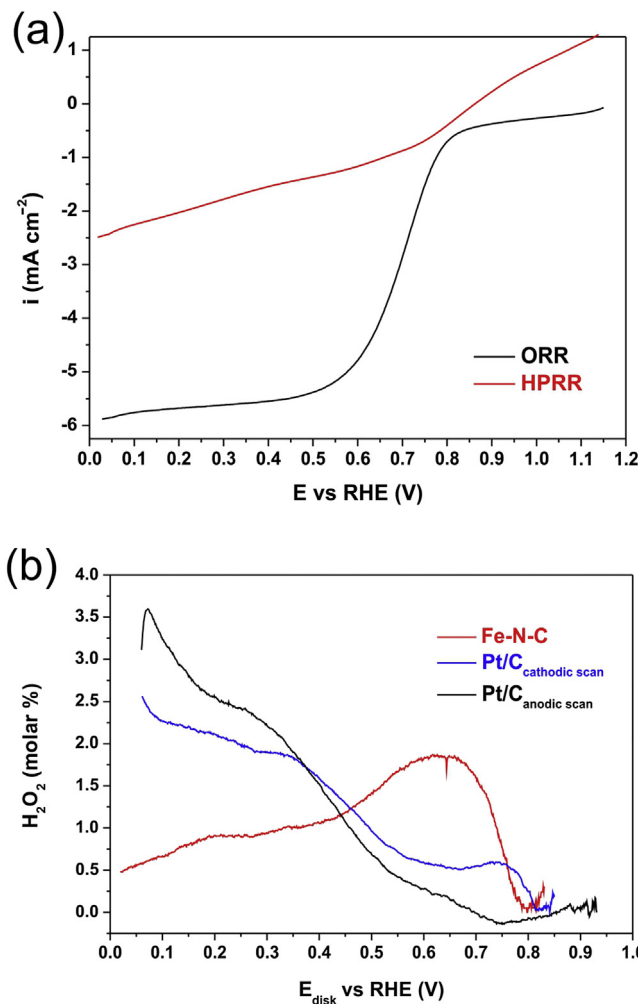


**Fig. 4.** (a) LSV recorded at 5 mV s<sup>-1</sup> and 1600 rpm in N<sub>2</sub>-saturated 0.5 M H<sub>2</sub>SO<sub>4</sub> with the addition of 1 mM H<sub>2</sub>O<sub>2</sub> for Fe-N-C catalyst. LSV in O<sub>2</sub>-saturated 0.5 M H<sub>2</sub>SO<sub>4</sub> (without H<sub>2</sub>O<sub>2</sub>) in the same conditions is also shown for comparison. (b) H<sub>2</sub>O<sub>2</sub> molar % calculated from the RRDE test measurements performed at 900 rpm in 0.5 M H<sub>2</sub>SO<sub>4</sub> for Fe-N-C and in 0.1 M HClO<sub>4</sub> for 20 wt.% Pt/C.

[51], they are comparable to similar Fe-N-C catalysts obtained by hard-templating method using silica sacrificial supports [9,36,59]. For this reason, we considered the Fe-N-C catalyst a potential good candidate to be tested in PEMFC. Moreover, the diffusion limiting current of our Fe-N-C catalyst almost corresponds to the limiting current of the Pt/C catalyst (see Fig. 3b).

Considering the  $i_0$  in the low overpotential region, the value for Fe-N-C is almost two orders of magnitude lower than for Pt/C catalyst (considering the anodic scan direction). Similar results are available in the literature [76]. In the high overpotential region the  $i_0$  value of Fe-N-C is still almost one order of magnitude lower than for Pt/C catalyst.

To investigate more in detail which is the predominant reaction pathway for ORR on the Fe-N-C catalyst, its activity toward the hydrogen peroxide reduction reaction (HPRR), in the absence of O<sub>2</sub>, was assessed. LSV was performed in deaerated electrolyte solution after the addition of H<sub>2</sub>O<sub>2</sub> in the concentration of 1 mM. This value was chosen because it is very close to the concentration of O<sub>2</sub> in saturated 0.5 M H<sub>2</sub>SO<sub>4</sub> solution [77], to compare the ORR activity with the HPRR activity of the catalyst. Moreover, this concentration is about the maximum H<sub>2</sub>O<sub>2</sub> concentration that can be found during ORR experiments in RDE [78]. As shown in Fig. 4a, in spite of the concentration of H<sub>2</sub>O<sub>2</sub> and O<sub>2</sub> were almost the same, the ORR current is almost three times higher compared to the HPRR current.

As evident from Fig. 4a, the increase in HPRR current with cathodic potential is almost linear, and the maximum reduction current is smaller than the limited diffusion currents expected for 1 mM H<sub>2</sub>O<sub>2</sub> from the Levich equation [79]. Similar results are available in the literature for heat-treated Fe-N-C ORR catalysts [64,79,80]. These results suggest that H<sub>2</sub>O<sub>2</sub> reduction is under kinetic control in all the considered potential range.

In comparison with the ORR, the kinetics of HPRR is sluggish, since it is never fast enough to completely reduce all the available flux of H<sub>2</sub>O<sub>2</sub>, even at high overpotentials. Moreover, part of the reduction current could be originated from H<sub>2</sub>O<sub>2</sub> chemical disproportionation [79]. However, this possibility is most likely excluded, as explained by Jaouen and Dodelet [78,79], letting us deduce that the observed current was due to HPRR. Interestingly, at high potentials the Fe-N-C catalyst shows a hydrogen peroxide oxidation current.

To deeper investigate the ORR pathway on the Fe-N-C catalyst, the RRDE test was also performed. Fig. 4b shows the results obtained in terms of H<sub>2</sub>O<sub>2</sub>% generated from the ORR. Equation (3) was used to calculate the% of H<sub>2</sub>O<sub>2</sub> produced [81]:

$$\% \text{H}_2\text{O}_2 = 100 \cdot \frac{\frac{2I_r}{N}}{I_d + \left(\frac{I_r}{N}\right)} \quad (3)$$

where  $I_d$  is the current at the disk,  $I_r$  is the current at the ring and  $N$  is the ring collection efficiency (44%).

The generation of H<sub>2</sub>O<sub>2</sub> for the Fe-N-C catalysts is between 0.5 and 2 molar % over the whole scanned potential range, evidencing a good selectivity towards a complete 4-electrons O<sub>2</sub> reduction to H<sub>2</sub>O. In particular, at potential values where the cathode of a PEMFC is mostly operating, that is, between 0.6 and 0.4 V vs RHE, the amount of H<sub>2</sub>O<sub>2</sub> generated is between 1 and 2%. Values of H<sub>2</sub>O<sub>2</sub>% production in the same order of magnitude were measured in acidic conditions by other groups for similar pyrolyzed catalysts containing Fe, N and C [64,79,82].

The 20 wt.% Pt/C catalyst was also analyzed for comparison. For this catalyst, at lower overpotentials (between 0.80 and 0.50 V vs RHE), the peroxide generation is lower than for our Fe-N-C catalyst, especially in the anodic potential scan direction, where the Pt particles' surface is free from oxide species. Otherwise, the peroxide production is higher in the cathodic scan direction, due to the presence of oxides on the Pt surface at these potentials, which hinders in some way the complete 4 e<sup>-</sup> oxygen reduction. This behavior is typical of Pt in acidic conditions [69,82,83]. However, a significant increase in the ring current for Pt/C catalyst was detected when the disk potential approached the H-underpotential deposition region [82].

From the results of these electrochemical tests in 3-electrodes RDE-RRDE cell, we can draw some conclusions about the ORR pathway on the Fe-N-C catalyst. First, we can deduce that the Fe-N-C catalyst is able to electro-reduce O<sub>2</sub> to H<sub>2</sub>O and to H<sub>2</sub>O<sub>2</sub>, but much less able to electro-reduce H<sub>2</sub>O<sub>2</sub> to H<sub>2</sub>O. As a consequence, since HPRR kinetics is considerably slower than the total (4 e<sup>-</sup>) and partial (2 e<sup>-</sup>) ORR kinetics, we can conclude that the sequential 2e<sup>-</sup>+2e<sup>-</sup> reduction mechanism with intermediate formation of H<sub>2</sub>O<sub>2</sub> is not the main catalytic ORR pathway on this catalyst. If it was occurring, it would be only marginal. In facts, if the sequential mechanism was predominant, the HPRR kinetics should have been higher, or at least comparable, to the ORR. However, this is not occurring, as demonstrated by the results in Fig. 4a. We can thus conclude that the direct 4 e<sup>-</sup> reduction mechanism is predominant. The partial 2 e<sup>-</sup> reduction of O<sub>2</sub> to H<sub>2</sub>O<sub>2</sub> is also occurring, as demonstrated by the RRDE test. These results underline how the presence of at least one of two types of active sites is essential, to improve the catalyst performance toward a complete reduction of O<sub>2</sub> to H<sub>2</sub>O, minimizing the H<sub>2</sub>O<sub>2</sub> generation. First, effective HPRR reduction

active ensembles are necessary to enhance at maximum the reduction of the peroxide generated by the partial  $2e^-$  mechanism, via the sequential  $2e^- + 2e^-$  mechanism. Second, active sites able to simultaneously bind the two O atoms of the dioxygen molecules are necessary to stabilize the  $H_2O_2$  intermediate in acidic media (avoiding its desorption in the bulk solution), to favor the direct  $4e^-$  pathway [82].

For DMFC application, one of the most important characteristic that an ORR electrocatalyst must possess is to be tolerant to the presence of methanol. As a matter of fact, the permeation of fuel from the anode to the cathode through the Nafion® proton-conducting membranes (crossover effect), is one of the major barriers to the wide-scale commercialization of DMFC devices [84]. If Pt is used as catalytic material for the cathode, it suffers a relevant deactivation due to the methanol crossover. In fact, the high activity of Pt towards MOR can easily occur at the high potentials usually present at the cathode of the DMFC. This causes a considerable decrease in the open circuit potential ( $E_{oc}$ ) because of the presence of both methanol and oxygen at the cathode, generating a mixed potential due to the fuel-oxidant mixture [38]. Another reason for decrease of the  $E_{oc}$  is the poisoning of Pt catalyst by the MOR intermediates [42,85]. As a consequence, the overall power density that the DMFC can generate remarkably decreases during operation [38,41]. The use of methanol-tolerant cathode catalysts is a good strategy to minimize this effect, and therefore increase the performance and the durability of DMFC.

As already demonstrated in the literature [9,86,87], the NNM catalysts containing Fe, N, and C do not exhibit any activity towards MOR. Therefore, we tested the ORR activity of Fe-N-C, in the presence of various methanol concentrations. The methanol concentrations were chosen in the range from a minimum of 0.01 to a maximum of 2 M, which is the concentration of the methanol solution used to feed the anode in the DMFC tests (see Section 3.3). Fig. 5a shows the results of the methanol tolerance test, while Fig. 5b shows the behavior of the 20 wt.% Pt/C catalyst with and without methanol, for comparison.

For the Fe-N-C catalyst, there is almost no difference between the LSV curves without methanol and with methanol in different concentrations. Consequently, the Fe-N-C has a high methanol tolerance, and the ORR is the predominant process at the Fe-N-C electrodes over the whole potential range. Only a very small negative shift of about 10 mV is observed in the mixed kinetic-diffusion control zone. This could be due to a slight decrease of the electrical conductivity and/or of the  $O_2$  solubility in the electrolyte solution containing methanol.

On the contrary, for the Pt/C catalyst, the effect of the presence of methanol during the LSV is much more evident, with a severe decrease in the performance. The MOR, rather than the ORR, was the preferred reaction on the Pt/C electrode. Consequently, in spite of the almost 100 mV higher potential of the Pt catalyst in the mixed kinetic-diffusion zone compared to Fe-N-C in the absence of methanol, with a methanol concentration of 0.1 M, a high peak of methanol oxidation appears. As a consequence, the Pt/C catalyst has a remarkable 350 mV decrease in the  $E_{1/2}$  of the ORR, making the performance of Fe-N-C much better than for Pt/C catalyst in these conditions.

### 3.3. DMFC test

#### 3.3.1. Cathode formulation optimization

The performance of the Fe-N-C catalyst was analyzed in a single DMFC fed with 2 M methanol and pure  $O_2$  at 90 °C. The first part of this study consisted in the optimization of the cathode catalyst layer. The parameters considered for the optimization were: i. the Nafion ionomer content in the dry catalytic layer, ii. the total cata-

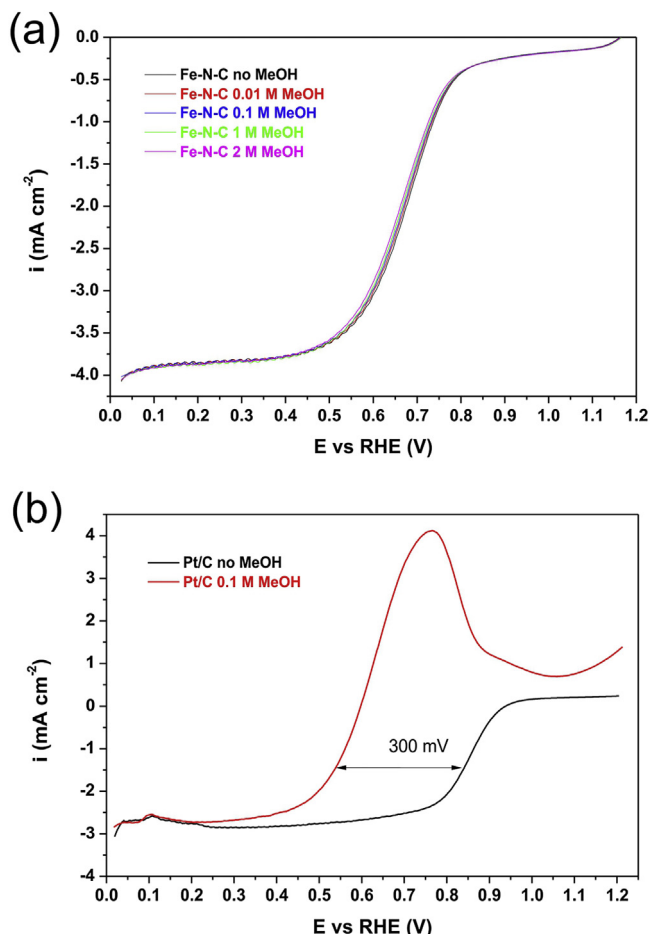


**Fig. 5.** LSV recorded in  $O_2$ -saturated 0.5 M  $H_2SO_4$  at 900 rpm and  $5 \text{ mV s}^{-1}$  in the presence of different methanol concentrations for the Fe-N-C catalyst (a) and for a commercial 20 wt.% Pt/C catalyst (b).

lyst loading, and iii. the carbon black (Vulcan) quantity mixed with Fe-N-C catalyst before deposition on the GDL.

First, preliminary tests were performed using pure Fe-N-C catalyst (without mixing with Vulcan) with different loadings and amounts of Nafion®. As evident from the results shown in Fig. 6a, the DMFC performance is low with the smallest amount of Nafion® employed (4 wt.%). This value was the same amount used for the anode catalyst layer preparation based on our previous results [38]. Increasing the amount of Nafion® to quantities more similar to the typical used in the literature for similar Fe-based NNM catalysts (i.e., between 35 and 50 wt.%) the performance increases considerably. In particular, comparing the results obtained with the same catalyst loading ( $2.5 \text{ mg cm}^{-2}$ ), the performance is better with the highest Nafion® content (50 wt.%). In fact, the Fe-N-C catalyst has high porosity, and thus needs a high ionomer quantity to maximize the connection of the protons with the electrolyte membrane. With 50% of Nafion®, two tests were made with different catalyst loadings ( $2.5$  and  $5 \text{ mg cm}^{-2}$ ), showing almost the same performance, even if with the lower catalyst loading the performance was slightly better. Thus, we can conclude that fabricating the cathode with too high amounts of the catalyst is not useful to increase the DMFC performance. As a consequence, the catalyst layer is affected by mass transport limitations. Possibly, in the presence of a thicker catalyst layer, the tortuosity of the reactants ( $H^+$  and  $O_2$ ) pathway increased too much, making the presence of more catalyst practically useless. The presence of such type of mass transport problematic can be found in the literature for similar NNM catalysts synthesized with a silica template method [59].

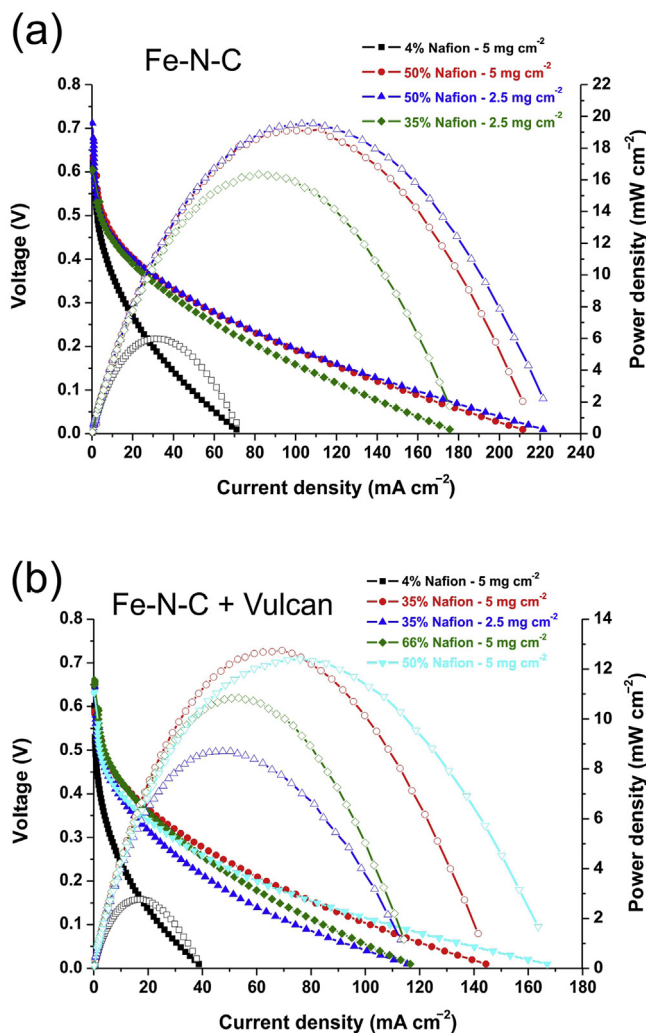


**Fig. 6.** Polarization curves (filled symbols) and power density curves (open symbols) of the  $4\text{ cm}^2$  single DMFC at  $90^\circ\text{C}$ . (a) Fe-N-C: different loadings and different Nafton® wt.% contents on the dry cathode. (b) Fe-N-C + Vulcan in 1:1 wt. ratio: different loadings and different Nafton® wt.% contents on the dry cathode.

In parallel, we also tested the DMFC using the Fe-N-C catalysts mixed in 1:1 wt. ratio with Vulcan carbon black. These tests were done to investigate the cathode behavior in the presence of additional carbon materials. In facts, some studies have been published with both Pt-based and NNM catalysts showing an improvement in fuel cell performance with the addition of carbon materials in different proportions to the catalytic layer [88–90]. These improvements in the performance could be ascribed to the changes the hydrophobicity of the catalyst layer, affecting water transport properties [29,30,90]. Another reason for such improvements could be the increasing in the electronic conductivity. In particular, the better performance for MEA prepared using NNM catalysts were obtained with Nafton® contents between 25 and 75 wt.% [9,90]. Such high ionomer contents could cause separation of the catalyst particles, breaking the electronic pathway and leading to loss of electronic conductivity. A possible way of compensation is to add conductive materials, such as carbon materials, to the catalyst before deposition onto the GDL. In fact, carbon can act as a bridge, interconnecting catalyst particles and reestablishing a continuous electronic pathway [91].

Comparing the results of the tests of the DMFC prepared with (Fig. 6b) and without Vulcan carbon black (Fig. 6a) addition to Fe-N-C at the cathode, there is no any improvement, suggesting that

for our Fe-N-C catalyst the carbon black addition is not useful to get better cell performances. In fact, considering the same total loading (Vulcan + Fe-N-C catalyst) on the GDL and the same Nafton® % content, the results obtained with only Fe-N-C are always better in terms of open circuit potential, power density, and current density. This could be explained by the presence of more catalyst (the double quantity) on the electrode for the case of pure Fe-N-C tests. Also considering only the total amount of Fe-N-C catalyst on the electrode (i.e.  $2.5\text{ mg cm}^{-2}$  of Fe-N-C and  $5\text{ mg cm}^{-2}$  of Fe-N-C + Vulcan 1:1 wt. ratio), the results obtained with the pure catalyst are better. This could be explained in terms of mass transport limitations in this catalyst occurring especially at high current densities [59]. Thus, we can conclude that the previous considerations about the addition of Vulcan in the catalytic layer are not valid in the case of our Fe-N-C catalyst. This could be due to its extremely high specific surface area and porosity [32], and to its good electrical conductivity. In fact, in spite of the high content of Nafton® ionomer in the dry electrode, the electrical conductivity is still good, and the accessibility of the reactants to the active sites is not limited.

**Table 2** summarizes the results of Fig. 6a–b in terms of cell open circuit potential, maximum current density, and maximum power density.

It is evident that the best results for the Fe-N-C catalyst as DMFC cathode were obtained with no Vulcan addition, 50 wt.% Nafton content and a catalyst loading of  $2.5\text{ mg cm}^{-2}$ . The maximum power density obtained in these conditions was  $19.6\text{ mW cm}^{-2}$ , which is close to the results obtained by other groups using similar Fe-N-C catalysts in similar testing conditions [9,25].

The test conditions leading to the better performance shown in Table 2 were then chosen hereafter as optimum conditions, and were used to perform the following DMFC short-term durability tests, as well as the  $\text{H}_2/\text{O}_2$  PEMFC test described afterwards in Section 3.4.

It is important to remark that to get the best MEA performance, any particular electrocatalyst developed requires a specific optimization to determine the most appropriate ionomer-to-catalyst ratio and catalyst loading on the electrode [90]. In fact, the ionomer transports  $\text{H}^+$  ions to active sites and helps to remove the  $\text{H}_2\text{O}$  generated from active sites. Generally, a higher ionomer content has a beneficial effect on the kinetics, due to the better ionic transport and conductivity, but it hinders the  $\text{O}_2$  mass transport especially at high current densities, causing blocking of the pores [92].

From the results in Table 2, both Nafton® amount and catalyst loading influence the  $E_{oc}$  of the cell: higher Nafton® contents and lower catalyst loadings result in slightly higher  $E_{oc}$ . This could be explained by the above-mentioned beneficial effect of the ionomer on the electrode kinetics. Moreover, lower catalyst loading results in a thinner electrode, which may favor the transport phenomena at the catalytic layer (including mass and charge transport), which may lead to slight differences in charge transfer phenomena at open circuit [9,59].

### 3.3.2. Short-term durability test

To assess the durability of Fe-N-C catalyst, a short-term durability test was performed on the MEA prepared with the cathode in the optimum conditions found in Section 3.1, for both the Fe-N-C and Pt/C catalysts. The cell potential was kept constant to  $0.4\text{ V}$ , which is a higher value compared to the literature [9,25,36]. At this potential, the oxidation of methanol intermediates is less favored, and the MEA is operating at more stressful conditions, which could cause a faster poisoning of the active surface of the anodic catalyst, with a consequent higher decay of the DMFC performance. Polarization curves were recorded every 30 min. The methanol flow rate was  $5\text{ mL min}^{-1}$  (5 times higher than the flow rate used for the polarization curves recorded in Section 3.3.1). The use of a higher flow rate should lead to an increase of the kinetics due to a higher

**Table 2**

Performance parameters for the DMFC tests (from Fig. 6a-b).

Vulcan content [wt.%]	Nafion content [wt.%]	Catalyst layer loading [mg cm <sup>-2</sup> ]	<i>E</i> <sub>oc</sub> [V]	<i>i</i> <sub>max</sub> [mA cm <sup>-2</sup> ]	<i>P</i> <sub>max</sub> [mW cm <sup>-2</sup> ]
0	4	5	0.62	71	6.0
0	35	2.5	0.61	176	16.3
0	50	5	0.63	211	19.2
0	50	2.5	0.71	222	19.6
50	4	5	0.60	39	2.8
50	35	2.5	0.65	115	9.3
50	35	5	0.59	144	12.7
50	50	5	0.63	167	12.4
50	66	5	0.66	117	10.8

**Table 3**

Performance parameters for DMFC stability tests in Fig. 7 for Fe-N-C and Pt/C catalysts used at the cathode.

Cathode catalyst	MeOH flow [mL min <sup>-1</sup> ]	time [h]	<i>E</i> <sub>oc</sub> [V]	<i>i</i> <sub>max</sub> [mA cm <sup>-2</sup> ]	<i>P</i> <sub>max</sub> [mW cm <sup>-2</sup> ]	Specific <i>P</i> <sub>max</sub> [W g <sub>Pt</sub> <sup>-1</sup> ]	<i>P</i> decrease [%]
Fe-N-C	1	0	0.71	222	19.6	19.6	–
Fe-N-C	5	0	0.56	180	13.8	13.8	–
Fe-N-C	5	0.5	0.52	155	10.5	10.5	24
Fe-N-C	5	1	0.52	142	9.2	9.2	33
Fe-N-C	5	1.5	0.51	132	8.3	8.3	40
Fe-N-C	5	2	0.50	124	7.5	7.5	46
Fe-N-C	5	3	0.50	117	7.0	7.0	49
Pt/C	1	0	0.61	274	30.9	15.5	–
Pt/C	5	0	0.52	163	18.7	9.4	–
Pt/C	5	2	0.42	54	4.5	2.3	76

flux of reactants to the anodic compartment [38]. However, this also causes an increase of the water and methanol diffusion through the membrane, maximizing the crossover effect and the flooding [30] in a relatively short-time. In fact, the methanol crossover is detrimental for Pt, and flooding is highly affecting the performance of Fe-N-C based catalysts [93]. Fig. 7a shows the results of this test, together with the curve recorded with 1 mL min<sup>-1</sup> methanol flow (from Fig. 6a) for comparison. Table 3 summarizes the cell performance parameters taken at different times of the test. The DMFC performance shows a considerable decrease immediately at the beginning of the test (*t*=0), just with the increase of the methanol flow rate. The maximum power density decreases of about 30% and the open circuit potential has a negative shift of 150 mV. Even if the Fe-N-C catalyst exhibits a high methanol tolerance (see Section 3.2), the increase of the diffusion of both methanol and water through the membrane could cause problems of water removal from the cathode (cathode flooding), especially at high current density values, where a higher amount of water is also generated at the cathode [30].

After the first hour of the test, a further important performance decrease is observed, with the maximum power density decreasing of 24% from the value at *t*=0, though the *E*<sub>oc</sub> decreases only 40 mV. Going on with the test, the cell shows a slower performance decrease, losing about 49% of its maximum power density after 3 h of test. Interestingly, the *E*<sub>oc</sub> remains almost constant, showing only a 60 mV negative shift between 0.5 and 2 h of test, and remaining almost constant during the last hour. This fact indicates that the DMFC deactivation should not be ascribed to problems related to the formation of a mixed potential (due to the methanol oxidation occurring at the cathode), as suggested by the methanol tolerance test. As previously discussed, the performance decrease could mainly be due to water management problems.

In particular, the higher flow rate of methanol caused a significant performance loss for the DMFC, even if Fe-N-C catalyst is highly methanol-tolerant. This is probably due to a severe flooding [30,94] occurring in particular inside the micropores, which represent the 50% of the total surface area of the Fe-N-C catalyst [32], and where the majority of the ORR active sites are located. Sebastián et al. performed a 100 h stability test on an MEA prepared using an NNM catalyst obtained by pyrolysis of Fe, N, and C precursors,

and obtained a similar trend in performance decay, detecting the major decrease within the first 3 h, and afterward the performance loss decelerates with time [9]. Considering the performance decay recorded by Sebastián et al. with a 100 h test, and our performance decay with only 3 h test, we can conclude that our short-term durability protocol can be considered as a fast alternative way to test the flooding capabilities of catalysts. Based on the results obtained, one can have fast feedback to change the physical properties of the catalyst, in order to improve the overall DMFC performance.

As a comparison, the same test was conducted for a single 4 cm<sup>2</sup> DMFC where the MEA was prepared using a 40 wt.% Pt/C commercial catalyst at the cathode (Pt loading 1 mg cm<sup>-2</sup>). Fig. 7b shows the results. In this case, the DMFC exhibits a considerably higher performance compared to the DMFC prepared using Fe-N-C catalyst at the beginning of the experiment, with a methanol flow of 1 mL min<sup>-1</sup> (30.9 vs 19.6 mW cm<sup>-2</sup> maximum power density). However, the initial *E*<sub>oc</sub> of the MEA with the Pt/C catalyst at the cathode is about 100 mV lower than the *E*<sub>oc</sub> of the MEA prepared with Fe-N-C (see Table 3), despite the ORR onset potential of a Pt/C catalyst in acidic conditions in absence of methanol is considerably higher compared to Fe-N-C. This confirms that using Pt/C as a cathodic catalyst, the DMFC suffer the presence of a mixed potential, due to methanol oxidation, causing a sharp performance decrease [37]. Simply by increasing the methanol flow rate, the performance of the MEA with the Pt/C cathode shows a decrease of about 40% in maximum power density, although remaining still better than the Fe-N-C results in the same conditions. The *E*<sub>oc</sub> also shows a considerably high decrease of about 110 mV, reaching a lower value than the Fe-N-C based DMFC in the same conditions. After 2 h of test, the performance decrease of the DMFC with Pt/C cathode is even more evident: the maximum power density decreased by 76% compared to the value at *t*=0, being much lower than for the Fe-N-C. Also, the *E*<sub>oc</sub> value drops down to 0.42 V, that is, 80 mV lower than for Fe-N-C.

The performance of the Fe-N-C cathode was better regarding the short-term durability test compared to that of Pt/C. The superior methanol tolerance of Fe-N-C is clearly observed working at 5 mL min<sup>-1</sup> flow rate. Even after 3 h, the polarization and power density curves of Fe-N-C are better compared to those of Pt/C after only 2 h. In particular, the drop in *E*<sub>oc</sub> for the DMFC based on Pt/C

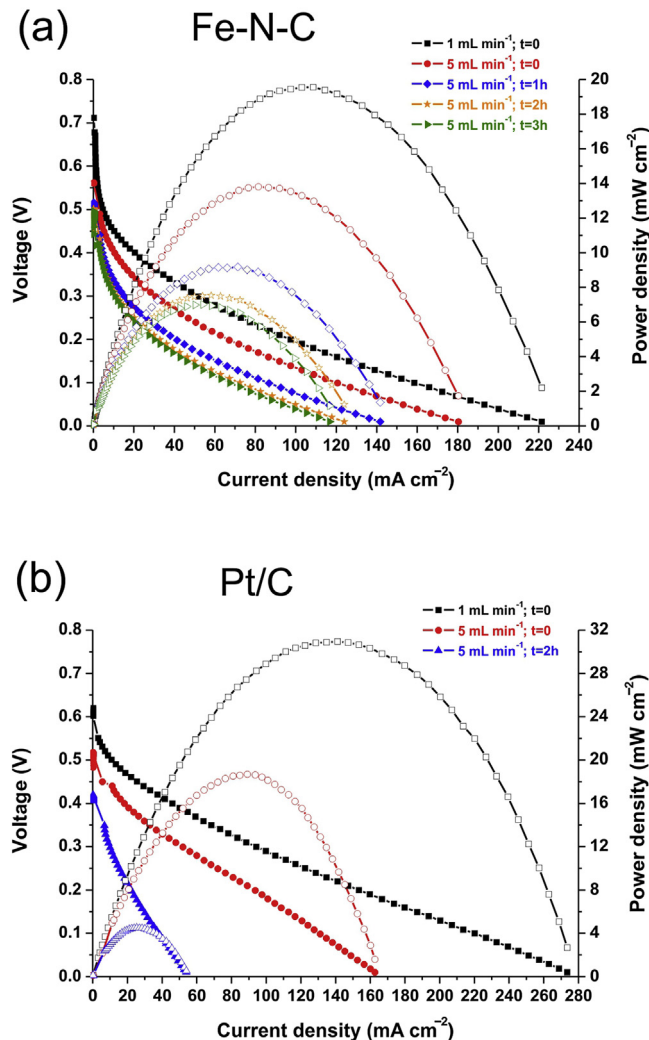


**Fig. 7.** (a) Performance of the  $4\text{ cm}^2$  single DMFC with Fe-N-C catalyst at the cathode along the durability test (potential kept constant at  $0.4\text{ V}$  for  $3\text{ h}$ ) at  $90^\circ\text{C}$  with  $5\text{ mL min}^{-1}$  methanol flow. The polarization curve with  $1\text{ mL min}^{-1}$  methanol flow is also shown for comparison. (b) Performance of the DMFC with commercial 40 wt.% Pt/C catalyst at the cathode tested in the same conditions.

cathode highlights the very detrimental effect of the methanol crossover on durability.

The use of an NNM catalyst at the cathode of a DMFC is convenient not only in terms of performances, but also from the economical point of view. As suggested by the maximum specific power density per g of total Pt used for the MEA fabrication (Table 3), the use of Fe-N-C catalyst leads to a considerable decrease of the total MEA cost. In fact, the main contribution to this cost is due to the Pt total content, being Ru about one order of magnitude and the NNM catalyst about two orders of magnitude cheaper than Pt [9]. In particular, the MEA fabricated with Pt/C as cathodic catalyst contains the double amount of Pt than the MEA fabricated with Fe-N-C (2 mg of total Pt per  $\text{cm}^2$  vs. 1 mg of total Pt per  $\text{cm}^2$ ).

Nevertheless, the performance of this Fe-N-C catalyst in DMFC is still low than what expected, leaving open space for future work in performance improvement. This could be achieved by both improving the stability of the catalyst active ensembles, and improving the structural features of the catalyst itself. This means, in turns, improving mass-transport properties to avoid, or at least limit, the flooding of micropores [29,30,95].

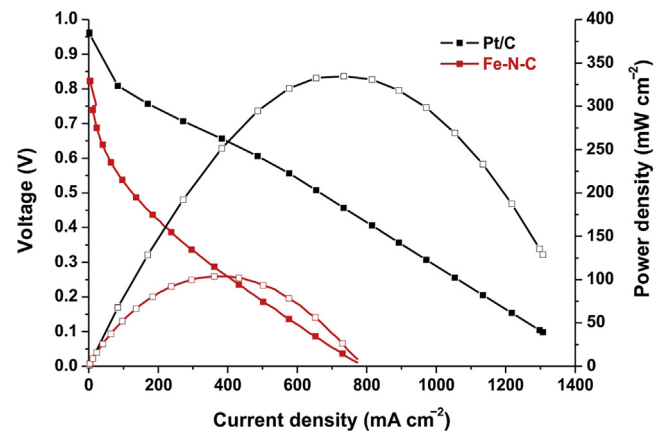


**Fig. 8.** Polarization (filled symbols) and power density curves (open symbols) measured at  $60^\circ\text{C}$  for a  $4\text{ cm}^2$  single  $\text{H}_2/\text{O}_2$  PEMFC prepared using Fe-N-C catalyst and a commercial 40 wt.% Pt/C catalyst at the cathode.

### 3.4. $\text{H}_2/\text{O}_2$ PEMFC test

Due to the promising results obtained in 3-electrodes cell and in DMFC, the performance of the Fe-N-C catalyst was also tested in a PEMFC fed with pure  $\text{H}_2$  and  $\text{O}_2$  at anode and cathode, respectively. Since the  $\text{H}_2$  crossover through the Nafion® proton conducting polymer is not a limiting factor in this type of fuel cells, to fabricate the MEA we used Nafion® 112 membrane (which is thinner than the Nafion® 117 used in DMFC tests), to minimize the ionic conduction resistance of the cell.

Fig. 8 shows the polarization and power density curves resulting from this test, together with the results of the same test performed using a commercial Pt/C catalyst instead of Fe-N-C at the cathode. The maximum power density recorded at  $60^\circ\text{C}$  for the cell made with Fe-N-C was  $105\text{ mW cm}^{-2}$ , which is about  $1/3$  than the maximum power density obtained with the Pt/C catalyst ( $335\text{ mW cm}^{-2}$ ) in the same testing conditions. However, if we normalize the maximum power density per g of total Pt used for the MEA fabrication, with Fe-N-C as cathode catalyst we obtain  $350\text{ W g}_{\text{Pt}}^{-1}$  (considering the  $0.3\text{ mg}_{\text{Pt}}\text{ cm}^{-2}$  used at the anode). For the MEA fabricated with Pt/C at the cathode, this value is  $372\text{ W g}_{\text{Pt}}^{-1}$  (considering the  $0.3\text{ mg}_{\text{Pt}}\text{ cm}^{-2}$  at the anode and the  $0.6\text{ mg}_{\text{Pt}}\text{ cm}^{-2}$  at the cathode). Concerning the open circuit potential ( $E_{\text{oc}}$ ), in the case of Pt/C it is around  $0.96\text{ V}$ , while for Fe-N-C catalysts the value is about  $140\text{ mV}$  lower, being around  $0.82\text{ V}$ . These values are in accordance with the  $E_{\text{on}}$  of  $0.93$  and  $0.83\text{ V}$  vs RHE that were obtained for the ORR polarization curve test in RDE (see Table 1). In fact, in the case of a PEMFC fueled with pure  $\text{H}_2$ , the anodic overpotential is very low, being the kinetics of HOR on Pt/C catalyst very fast [59,69]. Thus, all the activation potential losses in this case can be ascribed to the ORR overpotential.

Making a comparison of the performance of our Fe-N-C catalyst in this test with other results available in the literature for similar NNM catalysts is not easy, due to the non-uniformity of the experimental conditions adopted by the different research groups [96]. A collection of the best “state of the art” performances of NNM catalysts available in the literature measured in single  $\text{H}_2/\text{O}_2$  PEMFC is given by Monteverde Videla et al. [91]. There we can see that the highest power density performance values obtained for NNM catalysts as cathodic catalysts are as high as  $700\text{ mW cm}^{-2}$  at  $80\text{--}90^\circ\text{C}$  (while our test was performed at  $60^\circ\text{C}$ ). However, lower performances (around  $150\text{ mW cm}^{-2}$  at  $90^\circ\text{C}$ ) more similar to the results obtained with our Fe-N-C catalyst, can also be found in the literature [59,97,98]. The structural properties of the catalyst, such as the specific surface area and porosity appear to play important roles in

promoting effective mass transfer, especially at high current density [99].

#### 4. Conclusions

A methanol-tolerant Fe-N-C electrocatalyst for ORR with extremely high specific surface area and microporosity was synthesized using Fe(II)-phthalocyanine as single Fe, C, and N source, and SBA-15 silica as a sacrificial template. This catalyst showed very promising ORR activity in RDE-RRDE, together with a good selectivity towards a complete 4-electrons reduction to H<sub>2</sub>O via the direct reaction pathway. It was tested as cathode catalyst in DMFC. First, an optimization of the electrode formulation was made in terms of catalyst loading and Nafion content. Optimized tests in 4 cm<sup>2</sup> single cell DMFC allowed reaching 20 mW cm<sup>-2</sup> at 90 °C. A short-term durability test was performed, showing a deactivation of 64% in terms of maximum power density, which could be mainly ascribed to the flooding of the micropores and/or to the active ensembles deactivation. However, the performance loss of the Fe-N-C catalyst was considerably lower compared to a commercial Pt/C catalyst (which is highly affected by methanol crossover) after 3 h test, making the Fe-N-C catalyst a potential good candidate for Pt replacement in DMFC cathode. The performance in a PEMFC fueled with H<sub>2</sub> was tested as well, showing a performance of about 1/3 of the maximum power density achieved with a commercial Pt/C catalyst under the same testing conditions.

#### Acknowledgments

This work was supported by the Italian Ministry of Education, University and Research [PRIN NAMEDPEM, “Advanced nanocomposite membranes and innovative electrocatalysts for durable polymer electrolyte membrane fuel cells”, grant n. 2010CYTWAW]; the Madrid Regional Research Council (CAM) [RESTOENE-2 grant n. S2013/MAE2882]; the Spanish Economy and Competitiveness Ministry [ENE2013 grant n. 42322-R]. Mr. M. Raimondo and Dr. Marco Armandi from the Politecnico di Torino (Italy) are respectively acknowledged for FESEM images and FTIR measurements.

#### References

1. S. Specchia, C. Francia, P. Spinelli, Polymer electrolyte membrane fuel cells, in: J. Zhang, L. Zhang, H. Liu, A. Sun, R.-S. Liu (Eds.), *Electrochem. Technol. Energy Storage Convers.*, WILEY-VCH, Verlag, Weinheim, 2011, pp. 601–670.
2. Y. Feng, N. Alonso-Vante, *Phys. Status Solidi.* 245 (2008) 1792–1806.
3. J.M.R. Gallo, U.A. Icardi, V. Baglio, A. Corallini, A. Graizzaro, *Int. J. Hydrogen Energy* 36 (2011) 8082–8087.
4. A. Mehmood, M.A. Scibioh, J. Prabhuram, M.-G. An, H.Y. Ha, *J. Power Sources* 297 (2015) 224–241.
5. A. Stassi, C. D’Urso, V. Baglio, A. Di Blasi, V. Antonucci, A.S. Aricò, A.M. Castro Luna, A. Bonesi, W.E. Triaca, *J. Appl. Electrochem.* 36 (2006) 1143–1149.
6. S.K. Meher, G.R. Rao, *J. Phys. Chem. C* 117 (2013) 4888–4900.
7. A.S. Aricò, P.L. Antonucci, E. Modica, V. Baglio, H. Kim, V. Antonucci, *Electrochim. Acta* 47 (2002) 3723–3732.
8. P. Hernández-Fernández, S. Rojas, P. Ocón, J.L.G. de la Fuente, P. Terreros, M.A. Peña, J.L. García-Fierro, *Appl. Catal. B Environ.* 77 (2007) 19–28.
9. D. Sebastián, V. Baglio, A.S. Aricò, A. Serov, P. Atanassov, *Appl. Catal. B Environ.* 182 (2015) 297–305.
10. E. Negri, A.H.A.M. Videla, V. Baglio, A.S. Aricò, S. Specchia, G.J.M. Koper, *Appl. Catal. B Environ.* 166–167 (2015) 75–83.
11. A.H.A. Monteverde Videla, S. Ban, S. Specchia, L. Zhang, J. Zhang, *Carbon* 76 (2014) 386–400.
12. R. Jasinski, *Nature* 201 (1964) 1212–1213.
13. J.H. Zagal, A.P. Marita, J.F. Silva, *Fundamental aspects on the catalytic activity of metallomacrocyclics for the electrochemical reduction of O<sub>2</sub>*, in: J.H. Zagal, F. Bedioui, J.-P. Dodelet (Eds.), *N4-Macrocyclic Met. Complexes*, Springer, 2006, pp. 41–82.
14. C.W.B. Bezerra, L. Zhang, K. Lee, H. Liu, A.L.B. Marques, E.P. Marques, H. Wang, J. Zhang, *Electrochim. Acta* 53 (2008) 4937–4951.
15. Z. Chen, D. Higgins, A. Yu, L. Zhang, J. Zhang, *Energy Environ. Sci.* 4 (2011) 3167.
16. F. Jaouen, E. Proietti, M. Lefèvre, R. Chenitz, J.-P. Dodelet, G. Wu, H.T. Chung, C.M. Johnston, P. Zelenay, *Energy Environ. Sci.* 4 (2011) 114.
17. Non-Noble Metal Fuel Cell Catalysts, in: Z. Chen, J.-P. Dodelet, J. Zhang (Eds.), *WILEY-VCH*, Verlag, Weinheim, 2014.
18. L. Osmieri, A.H.A. Monteverde Videla, S. Specchia, *J. Power Sources* 278 (2015) 296–307.
19. R. Othman, A.L. Dicks, Z. Zhu, *Int. J. Hydrogen Energy* 37 (2012) 357–372.
20. S. Yuan, J.L. Shui, L. Grabstanowicz, C. Chen, S. Commet, B. Reprogé, T. Xu, L. Yu, D.J. Liu, *Angew. Chem. Int. Ed.* 52 (2013) 8349–8353.
21. A. Serov, K. Artyushkova, P. Atanassov, *Adv. Energy Mater.* 4 (2014) 1301735.
22. A.H.A. Monteverde Videla, L. Osmieri, M. Armandi, S. Specchia, *Electrochim. Acta* 177 (2015) 43–50.
23. J.Y. Cheon, T. Kim, Y. Choi, H.Y. Jeong, M.G. Kim, Y.J. Sa, J. Kim, Z. Lee, T.-H. Yang, K. Kwon, O. Terasaki, G.-G. Park, R.R. Adzic, S.H. Joo, *Sci. Rep.* 3 (2013) 2715, <http://dx.doi.org/10.1038/srep02715>.
24. A. Serov, K. Artyushkova, N.I. Andersen, S. Staripa, P. Atanassov, *Electrochim. Acta* 179 (2015) 154–160.
25. D. Sebastián, A. Serov, K. Artyushkova, P. Atanassov, A.S. Aricò, V. Baglio, *J. Power Sources* 319 (2016) 235–246.
26. B. Piela, T.S. Olson, P. Atanassov, P. Zelenay, *Electrochim. Acta* 55 (2010) 7615–7621.
27. L. Birry, J.H. Zagal, J.P. Dodelet, *Electrochim. Commun.* 12 (2010) 628–631.
28. N.A. Karim, S.K. Kamarudin, *Appl. Energy* 103 (2013) 212–220.
29. H. Li, Y. Tang, Z. Wang, Z. Shi, S. Wu, D. Song, J. Zhang, K. Fatih, J. Zhang, H. Wang, Z. Liu, R. Abouatallah, A. Mazza, *J. Power Sources* 178 (2008) 103–117.
30. A.H.A. Monteverde Videla, D. Sebastian, N.S. Vasile, L. Osmieri, A.S. Aricò, V. Baglio, S. Specchia, *Int. J. Hydrogen Energy* (2016), <http://dx.doi.org/10.1016/j.ijhydene.2016.06.060>.
31. J. Zeng, C. Francia, M.A. Dumitrescu, A.H.A. Monteverde Videla, V.S. Ijeri, S. Specchia, P. Spinelli, *Ind. Eng. Chem. Res.* 51 (2012) 7500–7509.
32. L. Osmieri, A.H.A. Monteverde Videla, M. Armandi, S. Specchia, *Int. J. Hydrogen Energy* (2016), <http://dx.doi.org/10.1016/j.ijhydene.2016.05.223>.
33. M. Ferrandon, A.J. Kropf, D.J. Myers, U. Kramm, P. Bogdano, G. Wu, C.M. Johnston, P. Zelenay, *J. Phys. Chem. C* 116 (2012) 16001–16013.
34. L. Osmieri, A.H.A. Monteverde Videla, S. Specchia, *J. Solid State Electrochem.* (2016), <http://dx.doi.org/10.1007/s10008-016-3332-2>.
35. A. Serov, U. Tylus, K. Artyushkova, S. Mukerjee, P. Atanassov, *Appl. Catal. B Environ.* 150–151 (2014) 179–186.
36. D. Sebastián, A. Serov, K. Artyushkova, J. Gordon, P. Atanassov, A.S. Aricò, V. Baglio, *ChemSusChem* (2016), <http://dx.doi.org/10.1002/cssc.201600583>.
37. R. Escudero-Cid, J.C. Pérez-Flores, E. Fatás, P. Ocón, *Int. J. Green Energy* 12 (2015) 641–653.
38. R. Escudero-Cid, M. Montiel, L. Sotomayor, B. Loureiro, E. Fatás, P. Ocón, *Int. J. Hydrogen Energy* 40 (2015) 8182–8192.
39. J.H. Kim, H.Y. Ha, I.H. Oh, S.A. Hong, H.N. Kim, H.I. Lee, *Electrochim. Acta* 50 (2004) 801–806.
40. H. Dohle, H. Schmitz, T. Bewer, J. Mergel, D. Stolten, *J. Power Sources* 106 (2002) 313–322.
41. R. Escudero-Cid, P. Hernández-Fernández, J.C. Pérez-Flores, S. Rojas, S. García-Rodríguez, E. Fatás, P. Ocón, *Int. J. Hydrogen Energy* 37 (2012) 7119–7130.
42. R. Escudero-Cid, A.S. Varela, P. Hernández-Fernández, E. Fatás, P. Ocón, *Int. J. Hydrogen Energy* 39 (2014) 5063–5073.
43. S. Shen, P.S. Chow, S. Kim, K. Zhu, R.B.H. Tan, *J. Colloid Interface Sci.* 321 (2008) 365–372.
44. D. Zhao, *Science* 279 (1998) 548–552.
45. J. Tao, J. Xiong, C. Jiao, D. Zhang, H. Lin, Y. Chen, *ACS Sustain. Chem. Eng.* 4 (2016) 60–68.
46. J. Xu, Y. Zhao, C. Shen, L. Guan, *ACS Appl. Mater. Interfaces* 5 (2013) 12594–12601.
47. S. Shrestha, W.E. Mustain, *J. Electrochem. Soc.* 157 (2010) B1665–B1672.
48. A.V. Ziminov, S.M. Ramsh, E.I. Terukov, I.N. Trapeznikova, V.V. Shamanin, T.A. Yurre, *Semiconductors* 40 (2006) 1131–1136.
49. F. Zheng, Y. Yang, Q. Chen, *Nat. Commun.* 5 (2014) 5261, <http://dx.doi.org/10.1038/ncomms6261>.
50. M. Wang, W. Yang, H. Wang, C. Chen, Z. Zhou, S. Sun, *ACS Catal.* 4 (2014) 3928–3936.
51. G. Wu, K.L. More, C.M. Johnston, P. Zelenay, *Science* 332 (2011) 443–447.
52. A. Ferrari, D. Basko, *Nat. Nanotechnol.* 8 (2013) 235–246.
53. I.-Y. Jeon, D. Yu, S.-Y. Bae, H.-J. Choi, D.W. Chang, L. Dai, J.-B. Baek, *Chem. Mater.* 23 (2011) 3987–3992.
54. H. Li, W. Kang, L. Wang, Q. Yue, S. Xu, H. Wang, J. Liu, *Carbon* 54 (2013) 249–257.
55. Y.W. Ma, Z.R. Liu, B.L. Wang, L. Zhu, J.P. Yang, X.A. Li, N. *Carbon Mater.* 27 (2012) 250–257.
56. F. Jaouen, A.M. Serventi, M. Lefèvre, J.-P. Dodelet, P. Bertrand, *J. Phys. Chem. C* 111 (2007) 5971–5976.
57. J.S. Zheng, X.Z. Wang, R. Fu, P. Li, D.J. Yang, H. Lu, J.X. Ma, N. *Carbon Mater.* 26 (2011) 262–270.
58. D. Geng, S. Yang, Y. Zhang, J. Yang, J. Liu, R. Li, T.K. Sham, X. Sun, S. Ye, S. Knights, *Appl. Surf. Sci.* 257 (2011) 9193–9198.
59. F. Jaouen, J. Herranz, M. Lefèvre, J.-P. Dodelet, U.I. Kramm, I. Herrmann, P. Bogdanoff, J. Maruyama, T. Nagaoaka, A. Garsuch, J.R. Dahn, T. Olson, S. Pylypenko, P. Atanassov, E.A. Ustinov, *ACS Appl. Mater. Interfaces* 1 (2009) 1623–1639.
60. C.H. Choi, M.W. Chung, H.C. Kwon, J.H. Chung, S.I. Woo, *Appl. Catal. B Environ.* 144 (2014) 760–766.
61. E. Frackowiak, F. Béguin, *Carbon* 39 (2001) 937–950.

[62] M.J. Bleda-Martínez, C. Peng, S. Zhang, G.Z. Chen, E. Moralloín, D. Cazorla-Amorós, *J. Electrochem. Soc.* 155 (2008) A672–A678.

[63] Y.C. Wu, D. Feng, W.F. Koch, *J. Solution Chem.* 18 (1989) 641–649.

[64] J. Chlistunoff, *J. Phys. Chem. C* 115 (2011) 6496–6507.

[65] B.N. Grgur, N.M. Marković, P.N. Ross, *Can. J. Chem.* 75 (1997) 1465–1471.

[66] A. Damjanovic, D.B. Sepa, *Electrochim. Acta* 35 (1990) 1157–1162.

[67] J. Bett, J. Lundquist, E. Washington, P. Stonehart, *Electrochim. Acta* 18 (1973) 343–348.

[68] A. Holewinski, S. Linic, *J. Electrochem. Soc.* 159 (2012) H864–H870.

[69] U.A. Paulus, T.J. Schmidt, H.A. Gasteiger, R.J. Behm, *J. Electroanal. Chem.* 495 (2001) 134–145.

[70] S.L. Gojković, S.K. Zecevic, R.F. Savinell, *J. Electrochem. Soc.* 145 (1998) 3713–3720.

[71] G.S. Kumar, M. Raja, S. Parthasarathy, *Electrochim. Acta* 40 (1995) 285–290.

[72] Q. He, S. Mukerjee, *Electrochim. Acta* 55 (2010) 1709–1719.

[73] N.M. Markovic, T.J. Schmidt, V. Stamenkovic, P.N. Ross, *Fuel Cells* 1 (2001) 105–116.

[74] J. Perez, E.R. Gonzalez, E.A. Ticianelli, *Electrochim. Acta* 44 (1998) 1329–1339.

[75] I.A. Pasti, N.M. Gavrilov, S.V. Mentus, *Int. J. Electrochem. Sci.* 7 (2012) 11076–11090.

[76] A. Muthukrishnan, Y. Nabae, T. Hayakawa, T. Okajima, T. Ohsaka, *Catal. Sci. Technol.* 5 (2015) 475–483.

[77] K.E. Gubbins, R.D.J. Walker, *J. Electrochem. Soc.* 112 (1965) 469–471.

[78] F. Jaouen, *J. Phys. Chem. C* 113 (2009) 15433–15443.

[79] F. Jaouen, J.-P. Dodelet, *J. Phys. Chem. C* 113 (2009) 15422–15432.

[80] S.L. Gojković, S. Gupta, R.F. Savinell, *Electrochim. Acta* 45 (1999) 889–897.

[81] P. Xu, W. Chen, Q. Wang, T. Zhu, M. Wu, J. Qiao, *RSC Adv.* 5 (2014) 6195–6206.

[82] N. Ramaswamy, S. Mukerjee, *Adv. Phys. Chem.* 2012 (2012) 1–17.

[83] D. van der Vliet, D.S. Strmcnik, C. Wang, V.R. Stamenkovic, N.M. Markovic, M.T.M. Koper, *J. Electroanal. Chem.* 647 (2010) 29–34.

[84] D. Sebastián, V. Baglio, S. Sun, A.C. Tavares, A.S. Aricó, *ChemCatChem* (2015), <http://dx.doi.org/10.1002/cctc.201403026>.

[85] A. Velázquez-Palenzuela, F. Centellas, J.A. Garrido, C. Arias, R.M. Rodríguez, E. Brillas, P.L. Cabot, *J. Power Sources* 196 (2011) 3503–3512.

[86] A. Serov, M.H. Robson, K. Artyushkova, P. Atanassov, *Electrochim. Commun.* 22 (2012) 53–56.

[87] A. Serov, M.H. Robson, M. Smolnik, P. Atanassov, *Electrochim. Acta* 109 (2013) 433–439.

[88] Z. Yang, M.R. Berber, N. Nakashima, *Electrochim. Acta* 170 (2015) 1–8.

[89] S.-Y. Lin, M.-H. Chang, *Int. J. Hydrogen Energy* 40 (2014) 7879–7885.

[90] S. Stariha, K. Artyushkova, A. Serov, P. Atanassov, *Int. J. Hydrogen Energy* 40 (2015) 14676–14682.

[91] A.H.A. Monteverde Videla, L. Osmieri, S. Specchia, Non-noble metal (NNM) catalysts for fuel cells: tuning the activity by a rational step-by-step single variable evolution, in: J.H. Zagal, F. Bedioui (Eds.), *Electrochem. N4 Macrocycl. Met. Complexes*, 1, 2016, pp. 69–102, <http://dx.doi.org/10.1007/978-3-319-31172-2> (Energy).

[92] J. Xie, F. Xu, D.L. Wood, K.L. More, T.A. Zawodzinski, W.H. Smith, *Electrochim. Acta* 55 (2010) 7404–7412.

[93] G. Zhang, R. Chenitz, M. Lefèvre, S. Sun, J.P. Dodelet, *Nano Energy* (2016), <http://dx.doi.org/10.1016/j.nanoen.2016.02.038>.

[94] R. Escudero Cid, J.L. Gómez de la Fuente, S. Rojas, J.L.G. Fierro, P. Ocón, *ChemCatChem* 5 (2013) 3680–3689.

[95] S. Litster, G. McLean, PEM fuel cell electrodes, *J. Power Sources* 130 (2004) 61–76.

[96] M. Shao, Q. Chang, J.-P. Dodelet, R. Chenitz, *Chem. Rev.* 116 (2016) 3594–3657.

[97] A.L. Mohana Reddy, N. Rajalakshmi, S. Ramaprabhu, *Carbon* 46 (2008) 2–11.

[98] A. Velázquez-Palenzuela, L. Zhang, L. Wang, P.L. Cabot, E. Brillas, K. Tsay, J. Zhang, *Electrochim. Acta* 56 (2011) 4744–4752.

[99] D. Zhao, J.-L. Shui, L.R. Grabstanowicz, C. Chen, S.M. Commet, T. Xu, J. Lu, D.-J. Liu, *Adv. Mater.* 26 (2014) 1093–1097.